Monthly Notices of the ROYAL ASTRONOMICAL SOCIETY

Mon. Not. R. Astron. Soc. **414,** 3307–3321 (2011) doi:10.1111/j.1365-2966.2011.18634.x

A broad-band X-ray view of the warm absorber in radio-quiet quasar MR 2251−178

J. Gofford,[1★] J. N. Reeves,[1,2] T. J. Turner,[2] F. Tombesi,[3,4] V. Braito,[5] D. Porquet,[6] L. Miller,[7] S. B. Kraemer[8] and Y. Fukazawa[9]

[1]*Astrophysics Group, School of Physical Sciences, Keele University, Keele, Staffordshire ST5 8EH*
[2]*Department of Physics, University of Maryland Baltimore County, Baltimore, MD 21250, USA*
[3]*Department of Astronomy and CREEST, University of Maryland, College Park, MD 20742, USA*
[4]*X-ray Astrophysics Laboratory, NASA/GSFC, Greenbelt, MD 20771, USA*
[5]*Department of Physics and Astronomy, University of Leicester, University Road, Leicester LE1 7RH*
[6]*Observatoire Astronomique de Strasbourg, Université de Strasbourg, CNRS, UMR 7550, 11 rue de l'Université, 67000 Strasbourg, France*
[7]*Department of Physics, University of Oxford, Denys Wilkinson Building, Keble Road, Oxford OX1 3RH*
[8]*Institute of Astrophysics & Computational Sciences, Department of Physics, The Catholic University of America, Washington, DC 20064, USA*
[9]*Department of Physical Sciences, Hiroshima University, 1-3-1 Kagamiyama, Higashi-Hiroshima, Hiroshima 739-8526, Japan*

Accepted 2011 March 2. Received 2011 March 1; in original form 2011 February 7

ABSTRACT

We present the analysis of a new broad-band X-ray spectrum (0.6–180.0 keV) of the radio-quiet quasar MR 2251−178 which uses both *Suzaku* and *Swift*/Burst Alert Telescope data. In accordance with previous observations, we find that the general continuum can be well described by a power law with $\Gamma = 1.6$ and an apparent soft excess below 1 keV. Warm absorption is clearly present, and absorption lines due to the Fe unresolved transition array, Fe L (Fe XXIII–XXIV), S XV and S XVI are detected below 3 keV. At higher energies, Fe K absorption from Fe XXV–XXVI is detected and a relatively weak (EW $= 25^{+12}_{-8}$ eV) narrow Fe Kα emission line is observed ($E = 6.44 \pm 0.04$ keV) which is well modelled by the presence of a mildly ionized ($\xi \lesssim 30$) reflection component with a low reflection fraction ($R < 0.2$). At least five ionized absorption components with $10^{20} \lesssim N_{\rm H} \lesssim 10^{23}$ cm^{-2} and $0 \lesssim \log \xi/{\rm erg\,cm\,s^{-1}} \lesssim 4$ are required to achieve an adequate spectral fit. Alternatively, we show that the continuum can also be fit if a $\Gamma \sim 2.0$ power law is absorbed by a column of $N_{\rm H} \sim 10^{23}$ cm^{-2} which covers ∼30 per cent of the source flux. Independent of which continuum model is adopted, the Fe L and Fe XXV Heα lines are well fit by a single absorber outflowing with $v_{\rm out} \sim 0.14c$. Such an outflow/disc-wind is likely to be substantially clumped ($b \sim 10^{-3}$) in order to not vastly exceed the likely accretion rate of the source.

Key words: galaxies: active – galaxies: individual: MR 2251−178 – X-rays: galaxies.

1 INTRODUCTION

It is now well established that the soft X-ray spectrum of at least half of all Seyfert 1 galaxies is characterized by regions of photoionized 'warm' absorption along the line of sight (Blustin et al. 2005; McKernan, Yaqoob & Reynolds 2007). Extensive studies of the local Seyfert population with *Chandra* and *XMM–Newton* have revealed that this warm absorber (WA) is an intricate array of narrow absorption lines, often seen to be moderately blueshifted with $v \sim$ 100–1000 km s^{-1}, from various ionization stages of abundant elements such as C, N, O, N, Mg, Si, S and Fe (e.g. Kaastra et al. 2000; Kaspi et al. 2002; Crenshaw, Kraemer & George 2003). Detailed modelling of the WA with photoionization codes such as XSTAR (Bautista & Kallman 2001) have shown that the absorbing material is typified by an ionization parameter in the range $\log \xi/{\rm erg\,cm\,s^{-1}} \sim$ 0–3, a column density of between $N_{\rm H} \sim 10^{20}$–10^{23} cm^{-2}, and most likely originate in a wind outflowing from the putative torus (Blustin et al. 2005) or the later stages of an accretion disc wind (Proga & Kallman 2004). Energetically, due to their low $v_{\rm out}$, soft X-ray WAs typically have kinetic luminosities to the order of ∼1 per cent of an active galactic nucleus' (AGN's) bolometric luminosity (e.g. Blustin et al. 2005) and are thus unlikely play an important role in terms of AGN feedback scenarios.

In addition, there is now also a large body of observational evidence for blueshifted absorption lines at rest-frame energies greater than 7 keV in many AGN (e.g. PG 1211+143, Pounds et al. 2003; PDS 456, Reeves, O'Brien & Ward 2003; NGC 1365, Risaliti et al. 2005; MCG -5-23-16, Braito et al. 2007; H 1413+117, Chartas et al. 2007; Mrk 766, Miller et al. 2007; NGC 3516, Turner et al. 2008; Mrk 509, Cappi et al. 2009; 3C 445, Reeves et al. 2010; Braito et al. 2011; Tombesi et al. 2010a,b). This absorption is generally

★E-mail: jag@astro.keele.ac.uk

© 2011 The Authors
Monthly Notices of the Royal Astronomical Society © 2011 RAS

Downloaded from http://mnras.oxfordjournals.org/ at NASA Goddard Space Flight Ctr on July 11, 2014

attributed to Fe XXV/XXVI in an outflowing accretion disc wind and requires both a high column density (i.e. $N_{\rm H} \sim 10^{23}$–10^{24} cm^{-2}), high ionization parameter (i.e. $\log \xi$/erg cm s^{-1} $\sim$ 3–6) and an outflow velocity $\sim$0.1 c.

Given the large outflow velocities, the resulting kinetic power of accretion disc winds can be a significant fraction of the bolometric luminosity of an active nucleus (e.g. Pounds & Reeves 2007; Tombesi et al. 2010b), and they may represent a driving mechanism for AGN feedback processes. Indeed, extrapolating the kinetic luminosity over a conservative active phase and outflow duty cycle for a given AGN, it is often found that the total mechanical output can be in excess of, or is at least very similar to, the binding energy of a reasonably sized galaxy bulge. Accretion disc winds could therefore be a possible explanation for the observed M–σ relation (Ferrarese & Merritt 2000; Gebhardt et al. 2000); where mass ejected from a radiatively driven accretion disc wind (e.g. King 2003) can move out into a host galaxy, sweeping up material until, once a critical black hole (BH) mass has been reached, the interstellar medium has been evacuated of material and both star formation and super-massive black hole (SMBH) growth cease (see King 2010, and references therein).

1.1 The radio-quiet quasar MR 2251−178

MR 2251−178 ($z = 0.064$; Canizares, McClintock & Ricker 1978; Bergeron et al. 1983) was first detected as a bright X-ray source during the *Ariel V* all-sky survey (Cooke et al. 1978) and subsequently identified as a radio-quiet quasar by Ricker et al. (1978) using *SAS-3* observations. The quasar is located on the outskirts of a cluster of approximately 50 galaxies (Phillips 1980) and is surrounded by a large extended nebula of diffuse gas which is characterized by [O III] emission in the optical (Bergeron et al. 1983). More recent observations have also noted similar extended emission in the X-ray band (Kaspi et al. 2004; Gibson et al. 2005). The source is observed to be a weak radio emitter, and has a Fanaroff–Riley type I (FR I) morphology.

The first detailed spectral study of MR 2251−178 in the X-rays was conducted by Halpern (1984), who noted that absorption in the soft X-ray band varied on time-scales of around 1 yr. The variability implied an order of magnitude increase in the absorption column and was attributed to the change in ionization of material along the line of sight. Historically, this is regarded as the first suggestion of an X-ray WA in an AGN.

Subsequent observations with *EXOSAT*, *Ginga* and *BeppoSAX* established that the broad-band X-ray spectrum of MR 2251−178 can be well described by a power law of photon index $\Gamma \sim 1.7$ which is absorbed by a column density of around a few $\times$ 10^{22} cm^{-2} (Pan, Stewart & Pounds 1990; Mineo & Stewart 1993), and a high-energy roll-over at around 100 keV (Orr et al. 2001). Mineo & Stewart (1993) also found that the ionization state of the absorbing material was strongly correlated with the source luminosity.

In the ultraviolet (UV), Monier et al. (2001) found absorption lines due to Lyα, N V and C IV blueshifted in the rest frame by $\sim$300 km s^{-1}. The C IV absorption was later shown by Ganguly, Charlton & Eracleous (2001) to vary over a period of roughly 4 yr which enabled the authors to deduce a maximum distance of $\sim$2.4 kpc between the absorption clouds and the continuum source.

Kaspi et al. (2004), using a series of *ASCA*, *BeppoSAX* and *XMM–Newton* observations which spanned 8.5 yr, confirmed that the continuum can be described by an absorbed power law of photon index $\Gamma \sim 1.6$ but found that it further required an additional soft excess at low X-ray energies. The *XMM–Newton* spectrum required at least two or three separate ionized absorbers with column densities in the range 10^{20}–10^{22} cm^{-2}, and had physical properties which appeared to vary between observations. This lead the authors to posit a scenario where absorption clouds were moving across the line of sight over the time-scale of 'several months'. Further UV absorption lines from C III, H I and O VI were detected in the *FUSE* spectrum, which were blueshifted with velocities similar to those found by Monier et al. (2001).

MR 2251−178 has also been observed by the *Chandra* High Energy Transmission Grating (HETG) which revealed evidence of a highly ionized, high-velocity (i.e. $v = -12700 \pm 2400$ km s^{-1}) outflow in the Fe K band (Gibson et al. 2005). Gibson et al. (2005) attributed this absorption to the Lyα line of Fe XXVI, and inferred that unless the absorber has a low covering fraction the mass-loss rate of MR 2251−178 is at least an order of magnitude larger than the accretion rate.

In this paper we present a new broad-band X-ray observation of MR 2251−178, using data obtained with both *Suzaku* and the *Swift* Burst Alert Telescope (BAT). We begin by discussing the data reduction process in Section 2, and then parametrize the broad-band spectrum in Section 3. In Section 3.2 we discuss the several absorption lines which are detected and determine their statistical significance, before performing a detailed modelling of the spectrum with the XSTAR photoionization code in Section 4. To calculate luminosities, a concordance cosmology with $H_0 = 71$ km s^{-1} Mpc^{-1}, $\Omega_\Lambda = 0.73$, and $\Omega_{\rm m} = 0.27$ (Spergel et al. 2003) was adopted.

2 THE *Suzaku* AND *Swift* OBSERVATIONS OF MR 2251−178

Suzaku (Mitsuda et al. 2007) observed MR 2251−178 in the X-ray imaging spectrometer (XIS) nominal pointing position for 287 ks between 2009 May 7 and May 10. Data are included from the XIS (Koyama et al. 2007) and from the PIN instrument of the hard X-ray detector (HXD; Takahashi et al. 2007), both of which were processed using version 2.3.12.25 of the *Suzaku* data reduction pipeline.

A complementary hard X-ray data set obtained with the *Swift*/BAT, which observed MR 2251−178 as part of the 58 month all sky survey (Baumgartner et al. 2010), is also included in our analysis. A summary of the observations is included in Table 1.

2.1 XIS data reduction

XIS data were selected in the 3 $\times$ 3 and 5 $\times$ 5 modes using *ASCA* grades 0, 2, 3, 4 and 6. Standard XIS screening criteria were applied such that data were excluded if taken: (1) within 436 s of passage through the South Atlantic Anomaly (SAA), (2) within an Earth elevation angle (ELV) $<5^\circ$, and/or (3) with Earth day-time elevation angles $<20^\circ$. Hot and flickering pixels were removed from the XIS images using the CLEANSIS script. Source spectra were extracted from within circular regions of radius 2.8 arcmin, and background spectra were extracted from offset annuli of the same radius with care taken to avoid the corners containing the Fe^{55} calibration sources. The redistribution matrix file and ancillary response file were generated using the tasks XISRMFGEN and XISSIMARFGEN, respectively.

After checking for consistency (see Section 3.1), spectra obtained from the two front-illuminated XIS 0 and XIS 3 detectors were combined into a single source spectrum (hereafter referred to as XIS-FI) using MATHPHA in order to maximize the signal-to-noise ratio (S/N). Data from the back-illuminated XIS 1 (hereafter XIS-BI) were not combined and were instead analysed separately.

Downloaded from http://mnras.oxfordjournals.org/ at NASA Goddard Space Flight Ctr on July 11, 2014

Table 1. Summary of observation parameters.

	Instrument	Date	Exposure (ks)	Count rate (s^{-1})	Flux ($\times 10^{-11}$ erg cm^{-2} s^{-1})	Obs. ID
Suzaku	XIS-FI	07/05/09	136924	2.037 ± 0.003	4.29[a]	704055010
	XIS-BI			2.534 ± 0.004	4.35[a]	
	HXD/PIN		103800	0.135 ± 0.003	5.48[b]	
	HXD/GSO		89228	<0.3	<4.80[c]	
Swift	BAT	–	–	$(14.5 \pm 0.3) \times 10^{-4}$	6.63[d]	N/A

[a]2–10 keV flux; [b]15–50 keV flux; [c]50–100 keV flux 90 per cent upper limit; [d]20–100 keV flux.

Only XIS data over the energy range 0.6–9.0 keV were included due to a degradation in S/N above 9.0 keV. Data were also ignored between 1.6 and 2.1 keV due to uncertainties associated with the Si K edges intrinsic to the detector assembly of the XIS instrument.

The background subtracted count rates during the observation were $2.037 \pm 0.003\,s^{-1}$ per CCD for the XIS-FI and $2.534 \pm 0.004\,s^{-1}$ in the case of the XIS-BI. The net exposure for the observation was 136.9 ks. All XIS spectra and corresponding response files were binned to sample the half width half-maximum (HWHM) energy resolution of the detectors (i.e. ~60 eV resolution at 6 keV). Counts were additionally grouped with GRPPHA to achieve a minimum of 50 count per energy bin to enable the use of χ^2 minimization, which was used for all subsequent spectral fitting.

2.2 HXD/PIN AND GSO data reduction

The HXD/PIN spectrum was extracted from the cleaned events files and was also processed according to the screening criteria described previously. The non X-ray background (NXB) was generated using the tuned event files made available by the HXD instrument team (Fukazawa et al. 2009) with a count rate of 0.461 ± 0.001 count s^{-1}. The cosmic X-ray background (CXB) was simulated using the form of Boldt (1987) and resulted in a CXB count rate of ~0.024 count s^{-1}. Simultaneous good time intervals were found for both the source spectrum and the NXB using the MGTIME task, and the NXB exposure time was increased by a factor of 10 to reduce the effects of photon noise. The NXB and CXB were combined with equal weight using the MATHPHA operation and subsequently subtracted from the source spectrum within XSPEC.

The background subtracted count rate in the HXD/PIN was 0.135 ± 0.003 count s^{-1}, corresponding to a 15–50 keV flux of 5.48×10^{-11} erg cm^{-2} s^{-1}. The net exposure time was 103.8 ks after detector dead time was taken into account with HXDDTCOR. Spectra were binned to a 5σ level above the background per bin from 15 to 50 keV.

For consistency we also reduced the data obtained with the HXD/GSO. The total (background subtracted) GSO exposure was 89.2 ks for a count rate of <0.3 count s^{-1}, which corresponds to 90 per cent upper limit on the 50–100 keV flux of $<4.8 \times 10^{-11}$ erg cm s^{-1}. Note that the GSO data were not used during spectral fitting and were used solely to check the consistency of the time-averaged *Swift*/BAT data set.

3 BROAD-BAND X-RAY SPECTRAL ANALYSIS

We performed a wide-band spectral analysis of MR 2251−178 in the 0.6–180 keV energy range using XSPEC v. 12.6.0*q* (Arnaud 1996) and HEASOFT v. 6.10. All fits were modified by a Galactic column of $N_{\rm H(Gal)} = 2.42 \times 10^{20}$ cm^{-2} (Dickey & Lockman 1990) which

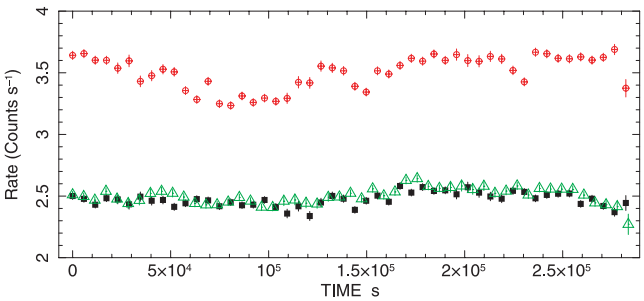

Figure 1. Lightcurves for the XIS0 (green triangles), XIS1 (red circles) and the XIS3 (black closed squares). Only small variations in the light curve were observed during the observations. 1σ error bars are roughly the size of the plot points.

was not allowed to vary. We used a photoelectric absorber with Wisconsin cross-sections (the wabs component in XSPEC; Morrison & McCammon 1983) to model the Galactic absorption. Spectral parameters are quoted in the rest frame of the source ($z = 0.064$) unless otherwise stated, and errors are quoted to the 90 per cent level for one parameter of interest (i.e. $\Delta\chi^2 = 2.71$). The cross-normalizations for the XIS-FI and XIS-BI were allowed to vary in all fits and generally found to be within ±2–3 per cent of each other. The HXD/PIN normalization was set to 1.16 of the XIS. The normalization on the *Swift*/BAT was left as a free parameter throughout, and was found to be 4–5 per cent greater than that of the XIS instruments. There was no strong variability (i.e. <10 per cent level) observed over the course of the observation. Lightcurves for the three XIS detectors are shown in Fig. 1. In all spectral plots XIS data are binned to sample the HWHM energy resolution of the detectors (i.e. 60 eV at 6 keV) unless otherwise stated.

3.1 Initial continuum parametrization

We first considered the X-ray spectrum of MR 2251−178 in the 3–5 keV band of the XIS data. An initial fit of the continuum with a simple power law of photon index $\Gamma = 1.56 \pm 0.01$ modified solely by Galactic absorption yielded a reasonable fit [with χ^2/degrees of freedom (d.o.f.) = 212.5/178]. Individually, the photon indices for the three XIS spectra are all in good agreement with this value, and have indices of $\Gamma = 1.55 \pm 0.01$, 1.55 ± 0.02 and 1.57 ± 0.02 for the XIS 0, XIS 1 and XIS 3 data, respectively.

Extending the data to include the full 0.6–180.0 keV energy range reveals significant deviations from the simple power-law fit and the fitting statistic is extremely poor (χ^2/d.o.f. = 4733.3/348). The residuals of this fit are shown in Fig. 2 (top panel). In the XIS data a clear soft excess can be seen at energies below around 0.7 keV, and there is a noticeable discrepancy between 0.8 and 1.6 keV, presumably due to the presence of the WA. The ubiquitous Fe Kα line

Downloaded from http://mnras.oxfordjournals.org/ at NASA Goddard Space Flight Ctr on July 11, 2014

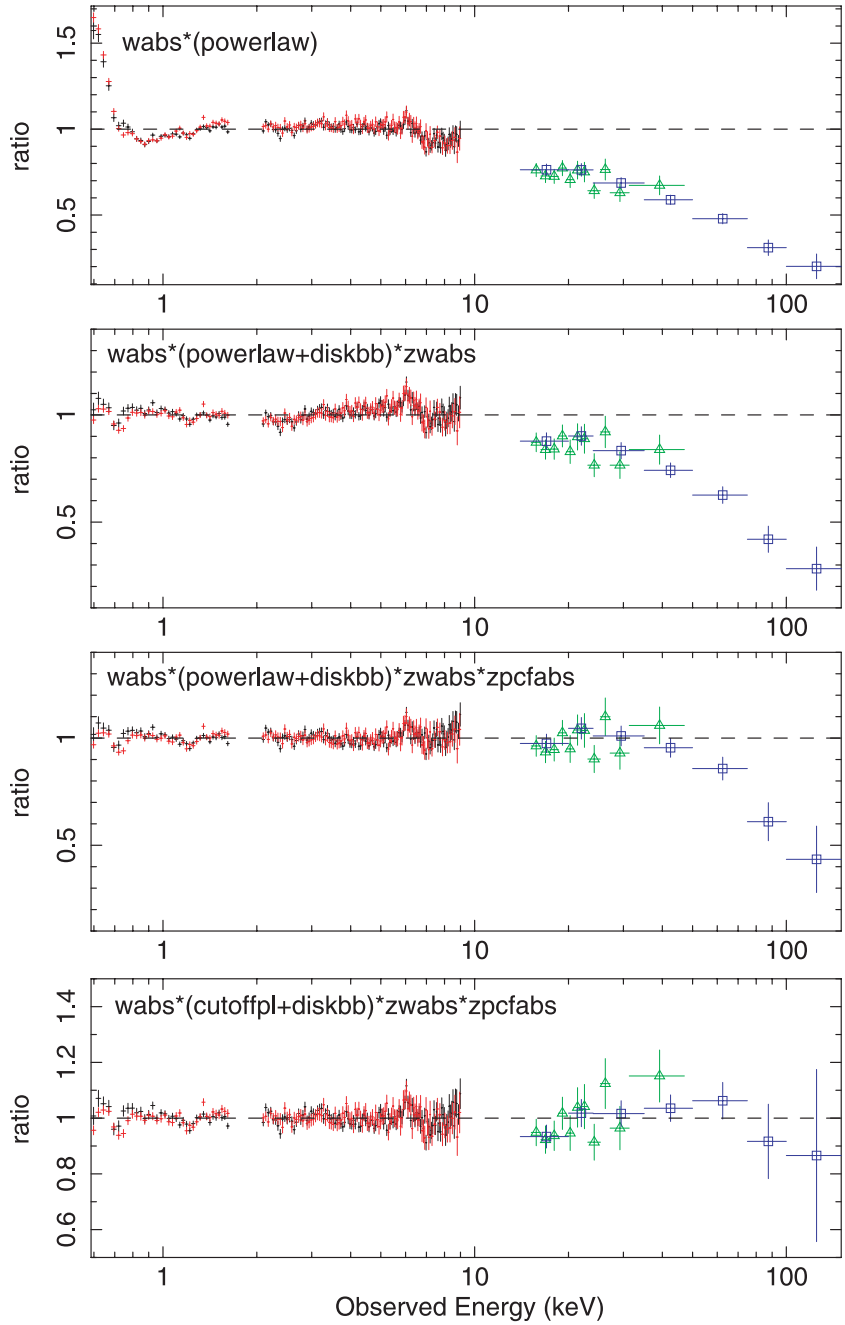

Figure 2. Broad-band data/model residuals of the *Suzaku* (XIS-FI: black, XIS-BI: red, PIN: green open triangles) and *Swift* (BAT: blue open squares) data when fitted with a variety of parametrizing models (Section 3.1). From top to bottom: (1) residuals when fitted solely by the 3–5 keV best-fitting power law; (2) residuals of the same data when fitted an accretion disc blackbody and power law absorbed by a fully covering neutral absorber; (3) as above, except with an additional partial-covering absorber included in the model and (4) as above, but with a cut-off power law. Note that the Fe Kα has not been fitted for illustrative purposes.

is also present at ∼6.4 keV. The spectrum also appears to roll over above 10 keV in accordance with the presence of the high-energy cut-off reported by Orr et al. (2001). Note that as the *Swift*/BAT spectrum is time-averaged over 58 months, we also checked the HXD/GSO spectrum to determine the validity of the high-energy cut-off present in the BAT data. We find a 90 per cent upper limit for the HXD/GSO flux of $<4.8 \times 10^{-11}$ erg cm^{-2} s^{-1} in the 50–100 keV band, which is consistent with the *Swift*/BAT flux over the same energy range (2.7×10^{-11} erg cm^{-2} s^{-1}) and suggests that the roll-over is valid for the *Suzaku* observation.

To parametrize the 0.6–180 keV continuum, we initially fit the data with a model of the form wabs × (powerlaw + diskbb + zgauss) × zwabs, where the diskbb component is a simple parametrization of the soft excess as an accretion disc blackbody, zgauss is a Gaussian used to model the Fe Kα fluorescence emission line and zwabs is a simple photoelectric absorber modelled in the source rest frame (i.e. at $z = 0.064$).

With this model the fit statistic is drastically improved, but is still quite poor (χ^2/d.o.f. = 1111.1/340). The power-law component has a photon index of $\Gamma = 1.67 \pm 0.01$ and is absorbed by

Downloaded from http://mnras.oxfordjournals.org/ at NASA Goddard Space Flight Ctr on July 11, 2014

Table 2. Summary of X-ray absorption and emission lines.

Line ID	$E_{\rm rest}$ (keV)	$E_{\rm lab}$ (keV)	Flux[a]	σ (eV)	EW (eV)	$\Delta\chi^2$[b]	MC (per cent)
Fe UTA	0.77 ± 0.01	0.729–0.775	$-241.0^{+67.0}_{-60.0}$	10[c]	-7 ± 2	65.6	>99.9
Fe XXIV (2s→3p)	1.29 ± 0.01	1.165	$-38.0^{+14.7}_{-11.3}$	<44	-4^{+2}_{-1}	66.1	>99.9
S XV	2.52 ± 0.02	2.461	-17.2 ± 5.7	10[c]	-6 ± 2	15.9	>99.9
S XVI	2.79 ± 0.03	2.623	$-11.5^{+4.7}_{-4.8}$	10[c]	-5 ± 2	10.9	>99.9
Fe Kα	$6.43^{+0.04}_{-0.03}$	6.4	$+14.0^{+6.7}_{-4.2}$	<117	$+25^{+12}_{-8}$	52.9	–
Fe XXV–XXVI	$7.57^{+0.2}_{-0.1}$	6.7 and/or 6.97	$-8.9^{+6.0}_{-4.7}$	183^{+185}_{-112}	-22^{+15}_{-11}	16.6	99.3

[a]Line flux quoted in units of $\times 10^{-6}$ erg cm^{-2} s^{-1}.
[b]Change in fitting statistics when adding a Gaussian to the best-fitting continuum model.
[c]Denotes that the parameter was fixed at a listed value.

$N_{\rm H} = 1.1 \times 10^{21}$ cm^{-2}, which is similar to that found by Ramìrez et al. (2008) for the lowly ionized absorber in the *Chandra*, Low Energy Transmission Grating (LETG) observation of this source. The accretion disc blackbody used to parametrize the soft excess has a temperature $kT = 62^{+1}_{-3}$ eV. An unresolved ($\sigma < 391$ eV) Fe Kα line is present at a rest-frame energy of $6.43^{+0.04}_{-0.03}$ keV which is consistent with an origin in neutral or mildly ionized material. As shown in Fig. 2 (second panel), the poor fit statistic is due to the model being unable to adequately reproduce the spectral curvature between ∼2–6 keV and in the hard X-ray band. This suggests that additional absorption is required.

We therefore tested for a more complex absorption scenario by adding an additional neutral absorber with $N_{\rm H} = 8.7^{+0.6}_{-0.7} \times 10^{22}$ cm^{-2} which covers 25 ± 1 per cent of the source flux (modelled with zpcfabs in XSPEC). This gives a significant improvement to the fit (χ^2/d.o.f. = 565.5/338 for two additional free parameters) and the residual spectral curvature in the XIS data is no longer present. With a softer photon index of $\Gamma = 1.83 \pm 0.01$, the new model was also able to replicate the observed flux in the HXD/PIN data. Nevertheless, the model is still unable to reproduce the curvature present in the *Swift*/BAT data (Fig. 2, third panel).

In order to fit the observed roll-over in the *Swift*/BAT data, we replaced the power law with a cutoffpl component which models a power law with an exponential high-energy cut-off ($E_{\rm cut}$). The addition of the cut-off further improves the fit by $\Delta\chi^2 = 63.2$ for one more free parameter, and there are no longer any residuals in the BAT data (Fig. 2, bottom panel). In this model $\Gamma = 1.72 \pm 0.03$ and $E_{\rm cut} = 116^{+31}_{-21}$ keV, zwabs has $N_{\rm H} = (1.1 \pm 0.1) \times 10^{21}$ cm^{-2}, zpcfabs covers 17 ± 2 per cent of the source flux with $N_{\rm H} = 9.9^{+1.3}_{-1.2} \times 10^{22}$ cm^{-2} and the soft excess is parametrized by a $kT = 57 \pm 2$ eV accretion disc blackbody. The final fit statistic is χ^2/d.o.f. = 502.3/337 and is our best-fitting continuum parametrization.

3.2 Absorption lines

Several absorption features are present below 3 keV and in the Fe K band. We modelled these absorption lines with Gaussian profiles fit in the rest frame of the AGN. The statistical significances for each absorption line in this section were determined against the best-fitting continuum model discussed above. Monte Carlo (MC) simulations were also performed to further assess the statistical significances; the details of which are discussed in Section 3.3. Table 2 shows a summary of all line parameters. Detailed discussion regarding all line identifications, including the consideration of alternative identifications, is presented in Appendix A.

3.2.1 The soft X-ray band

Below 2 keV two absorption lines are required (Fig. 3; top panel). The first is unresolved and detected at a rest-frame energy of $E = 0.77 \pm 0.01$ keV. This is consistent with the Fe I–XVI M-shell unresolved transition array (UTA) which is expected between 0.729 and 0.775 keV (Behar, Sako & Kahn 2001; Netzer 2004). The line has an equivalent width (EW) of -7 ± 2 eV and its addition to the model improves the global fit by $\Delta\chi^2 = 65.6$. The line is also >99.9 per cent significant from MC simulations.

The second line has a rest energy of 1.29 ± 0.01 keV and an EW $= -4^{+2}_{-1}$ eV. The line is highly significant (>99.9 per cent from MC simulations) and its addition improves the fit by $\Delta\chi^2 = 66.1$. Unlike the UTA, this second line does not have an energy that corresponds to any expected strong X-ray transitions. There are several possible identifications for this line (see Appendix A) but the most conservative association which is internally consistent with our XSTAR model (Section 4) is with the Fe XXIV 2s→3p doublet which is expected at a mean energy of $E = 1.165$ keV. This identification requires a blueshift of $v_{\rm out} = 0.11 \pm 0.01c$ (33000 ± 3000 km s^{-1}).

Two further Gaussian absorption lines are required at $E = 2.52 \pm 0.02$ and 2.79 ± 0.03 keV in the rest frame, with EWs of -6 ± 2 eV and -5 ± 2 eV, respectively (Fig. 3; middle panel). Both lines are significant at the >99.9 per cent level from MC simulations and their addition improves the model by a further $\Delta\chi^2 = 15.9$ and $\Delta\chi^2 = 10.9$, respectively. Theoretically, the strongest spectral features expected in the 2–3 keV energy range are those associated with the 1s→2p transitions of S XV ($E = 2.461$ keV) and S XVI ($E = 2.623$ keV), but the rest-frame energies of the detected lines do not correspond to either of these, suggesting that they may be blueshifted. If identified with the S XV and S XVI transitions, the measured line centroids indicate that they are blueshifted by $v_{\rm out} = 0.02 \pm 0.01c$ (6000 ± 3000 km s^{-1}) and $0.07 \pm 0.01c$ (21000 ± 3000 km s^{-1}), respectively. Both lines are unresolved and their widths were fixed to $\sigma = 10$ eV throughout.

3.2.2 The Fe K region

There are further residuals in the data/model ratio present in the Fe K region. In addition to the Fe Kα emission line, there is a clear broad absorption feature in the 6.5–8 keV range, as can be seen in the bottom panel of Fig. 3. Note that this absorption is found in excess of the neutral Fe K absorption edge (expected at $E = 7.1$ keV) which is included as part of both the zwabs and zpcfabs absorbers. This absorption trough was initially modelled with a broad Gaussian profile and its centroid energy left as a free parameter. The centroid

Downloaded from http://mnras.oxfordjournals.org/ at NASA Goddard Space Flight Ctr on July 11, 2014

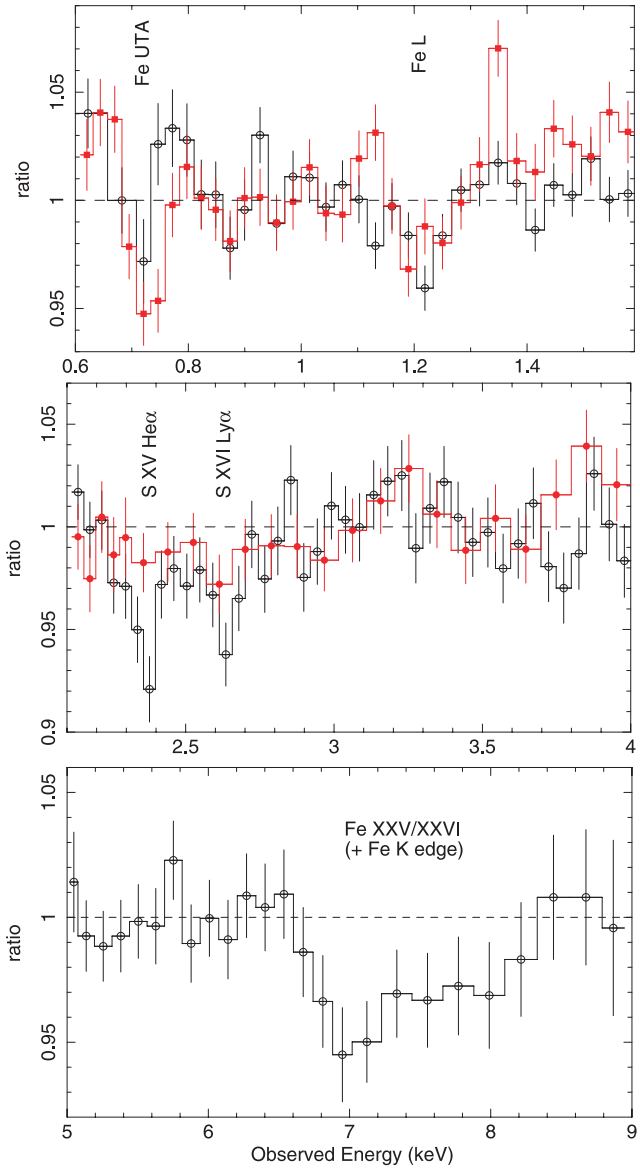

Figure 3. XIS-FI (black open circles) and XIS-BI (red closed circles) residuals when fit with the best-fitting continuum parametrization, as discussed in Section 3.1. The positions of the absorption lines are clearly labelled. The XIS-BI data have been omitted in the bottom panel due to reduced S/N at Fe K and the remaining XIS-FI data have been additionally binned by a factor of 3 above the HWHM energy resolution of the detectors for clarity.

energy and intrinsic width of the broad line are $E = 7.57^{+0.19}_{-0.12}$ keV and $\sigma = 209^{+244}_{-108}$ eV, and it has an EW of -26^{+18}_{-12} eV. The addition of the line results in a $\Delta\chi^2$ improvement of 16.6 for three additional free parameters, and it is statistically required at the 99.3 per cent level from MC simulations. With the addition of the broad absorption component, the width of the Fe Kα emission line is now more tightly constrained than before at $\sigma < 117$ eV (while EW $= 25^{+12}_{-8}$ eV).

In this energy range, the spectrum is expected to be dominated by atomic features attributable to iron. In particular, the 1s→2p transitions are expected to be particularly strong, as are the many resonance transitions associated with the Fe K edge near 7.1 keV (Kallman et al. 2004). If due to the strong 1s→2p transitions, this immediately places a constraint on the possible identifications for

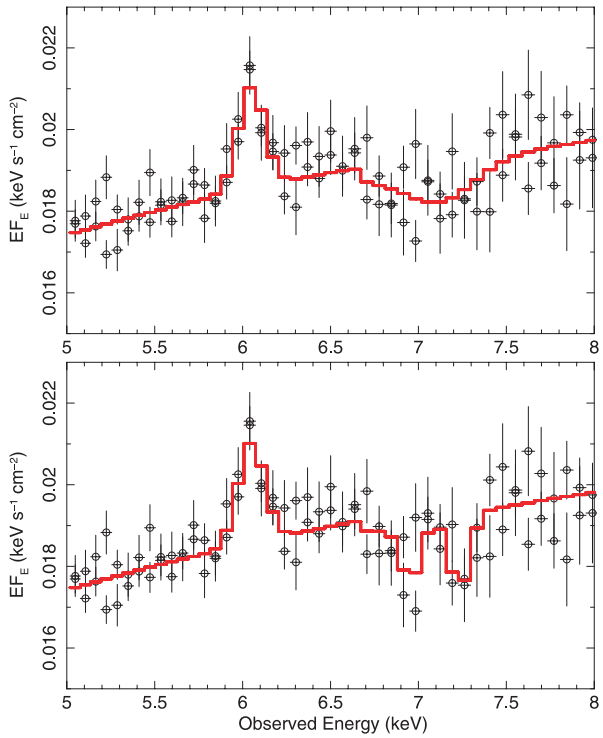

Figure 4. Plots showing the Fe K band. Top: the absorption feature fit with a broad Gaussian. Middle: the same absorption feature when fit as two separate Gaussian lines using the method outlined in Section 3.2.2.

the absorption as being due to at least Fe XVIII ($E \sim 6.5$ keV), where the Fe ions become sufficiently ionized to have an L-shell vacancy for a 1s electron transition. Above this ionization state, the 1s→2p transitions occur between $E \sim 6.5$–6.6 keV for Fe XVIII–XXIV, and at $E \sim 6.7$ keV and $E \sim 6.97$ keV for Fe XXV Heα and Fe XXVI Lyα, respectively. If the broad profile is identified with Fe XXV Heα, it requires a velocity shift of $v_{\rm out} = 0.13^{+0.03}_{-0.02}c$ ($= 39000^{+9000}_{-6000}$ km s^{-1}), while if identified with Fe XXVI Lyα the velocity shift is slightly lower at $v_{\rm out} = 0.10^{+0.03}_{-0.02}c$ (30000^{+9000}_{-6000} km s^{-1}).

An alternative interpretation is that the broad absorption represents a blend of the above lines rather than a single discrete profile. To investigate the possibility that the profile is a blend of He- and H-like Fe, we replaced the broad profile with two narrow ($\sigma = 50$ eV) absorption lines at fixed rest-frame energies of 6.7 and 6.97 keV and left their common velocity shift as a free parameter. This fit was a slight improvement to that of the broad Gaussian obtained previously, and gives a $\Delta\chi^2 = 18.1$ for three parameters of interest. Even so Fig. 4 shows that this model slightly underpredicts the absorbed flux of the Fe XXV Heα line at $E = 7.36^{+0.09}_{-0.11}$ keV (rest frame; $E = 6.92$ observed), while the Fe XXVI Lyα line is well fit. The resulting simultaneous velocity shift is $v = 0.10 \pm 0.01c$ with respect to the rest frame of the AGN.

3.3 Monte Carlo simulations

The MC simulations we used are analogous to those carried out by Tombesi et al. (2010a).

(i) We simulated $S = 1000$ XIS spectra between 0.6 and 10.0 keV based upon the baseline continuum parametrization model (outlined in Section 3.1), using the fakeit command in XSPEC. Both the HXD/PIN and *Swift*/BAT spectra were not included in the simulation as they had no effect on the absorption line parameters.

Downloaded from http://mnras.oxfordjournals.org/ at NASA Goddard Space Flight Ctr on July 11, 2014

(ii) In each of the simulated spectra, we stepped an inverted Gaussian of a set fixed width (see below) between two pre-defined energy bands in equal steps. After each step, the model was fitted for the line normalization of the Gaussian and the resulting overall $\Delta\chi^2$ was recorded. To sample the entire XIS spectrum, we performed this process twice, once to cover the Fe K band and once to cover the soft X-rays. For the Fe K absorption, we stepped a broad absorption line of $\sigma = 200$ eV width every 100 eV between 4 and 9 keV, while in the soft X-ray band we stepped a narrow absorption line of 10 eV width every 25 eV between 0.6 and 4 keV. Due to the XIS-BI having poorer S/N around Fe K, we used only the XIS-FI data in this band. Both the XIS-FI and XIS-BI were used in the soft X-rays where the S/N of the XIS-BI is higher.

(iii) After S spectra were generated the associated grid of χ^2 values then corresponded to how statistically likely it would be for a randomly occurring feature to have a $\Delta\chi^2$ improvement greater than a particular value. To assess the probabilities of the absorption lines detected, the $\Delta\chi^2$ value we obtained from our Gaussian fits was then compared to this generated grid of values. If N of the simulated spectra had a feature of significance greater than this $\Delta\chi^2$ value, the resulting detection confidence level of the measured line was $1 - N/S$.

The statistical probabilities for each line from MC simulations are recorded in Table 2.

4 SELF-CONSISTENT MODELLING

With both the general continuum and the absorption lines parametrized, we proceeded to replace the simple parametrizing models (i.e. zpcfabs and zwabs) with a series of self-consistent model grids generated using the XSTAR photoionization code. Each XSTAR grid contains a series of models, each pertaining to a particular photoionized spectrum with a characteristic ionization parameter (ξ), a column density ($N_{\rm H}$), and a redshift (z). In addition, each grid is attributed an intrinsic turbulent velocity ($V_{\rm turb}$) upon generation which determines the intrinsic width of any emission and absorption lines. The grid is then used as a simple multiplicative model in XSPEC to simultaneously fit the broad-band continuum and any spectral lines which may be present.

4.1 Fully covering models

We first modelled the spectrum assuming that the photoionized absorbers fully cover the view to the ionizing source, and that the soft excess represents an intrinsic component of the source continuum. We sequentially added XSTAR grids to a baseline continuum model of the form wabs × (cutoffpl+ diskbb+zgauss) × xstar until an acceptable fit had been achieved. Solar abundances of Grevesse & Sauval (1998) are assumed throughout unless otherwise stated.

4.1.1 Lowly ionized absorbers

In the soft X-ray band, two low turbulence ($v_{\rm turb} = 200\,{\rm km\,s^{-1}}$) ionized absorption components are required to provide a good description to both the Fe UTA absorption line and the general spectral curvature below 10 keV (see Fig. 5). The first absorber (Zone 1; $\Delta\chi^2 = 93.7$ for three additional free parameters) is lowly ionized and mainly responsible for the Fe UTA, while the second absorber (Zone 2) is less significant to the fit ($\Delta\chi^2 = 36.9$ for two more free parameters) and mainly fits the curvature. These absorbers also contribute to a shallow Fe K edge in the Fe K band, however its depth is insufficient to adequately replicate the feature (see Section 4.1.4). For fitting purposes the soft X-ray absorbers were assumed to be co-spatial and their common outflow velocity was fixed to $v_{\rm out} = 300\,{\rm km\,s^{-1}}$ to be consistent with the UV outflows reported in this source by Monier et al. (2001). Allowing the outflow velocities to vary did not yield any appreciable change in the fit statistic and they were thus left fixed throughout.

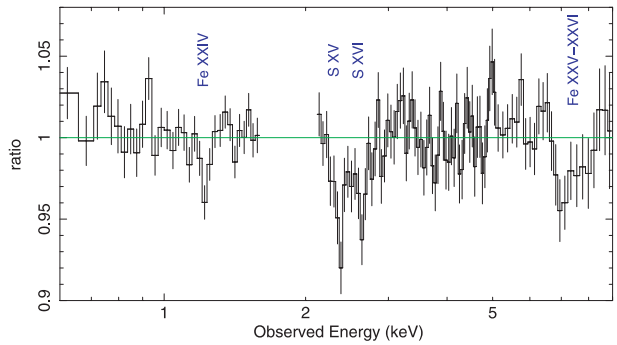

Figure 5. Data/model residuals of the XIS-FI data when fitted with two lowly ionized soft X-ray absorbers. The position of the Fe L, S XV, S XVI and Fe K absorption is clearly apparent. For clarity, the XIS-BI data have again been omitted. Data between 1.6 and 2.1 keV have been removed due to the instrumental Si K edge. See text for further details.

4.1.2 Detection of a Fe L-shell and Fe XXV absorber?

To model the absorption line at ∼1.29 keV, we used a higher turbulence ($v_{\rm turb} = 5000\,{\rm km\,s^{-1}}$) grid to account for the apparent line broadening. Zone 3 ($\Delta\chi^2 = 74.0$; see Table 3 for parameters) fits both the 1.29 keV line (Fig. 6) and also appears to fit the higher energy component of the Fe K absorption (Fig. 7) at $E \sim 7.7$ keV (rest frame; 7.24 keV observed). The outflow velocity found for this absorber is consistent with an identification of the Fe K absorption with Fe XXV Heα, however, the velocity is substantially larger than that found if the 1.29 keV line is identified as solely Fe XXIV. This could be the result of the line at 1.29 keV being a blend of Fe XXIII (2s→3p; expected at 1.127 keV) and Fe XXIV (2s→3p). If this is the case, the outflow velocity would then be consistent with that found for the XSTAR grid. We hereafter denote this absorption component the 'Fe L-shell absorber' as at an ionization of $\log\xi/{\rm erg\,cm\,s^{-1}} = 3.02$, the most prominent ions are from Fe XXIII–XXV.

4.1.3 Sulphur absorbers

There is a level of ambiguity regarding the correct physical interpretation of the lines at 2.52 and 2.79 keV. In particular, we were unable to obtain a satisfactory fit to the lines assuming solar abundances, and the lack of other distinct absorption lines meant that, when fit with variable abundances, the required Sulphur overabundance was entirely unconstrained. With the current data we therefore parametrize the absorption lines using a column density comprising solely of Sulphur ($N_{\rm S}$).

As discussed in Section 3.2.1, the most conservative interpretation is that the lines are identified with the 1s→2p transitions of He- and H-like sulphur, respectively. In this interpretation, the lines are well modelled by the addition of two further ionized absorbers. The first (Zone 3), which models S XV at ∼2.5 keV, is described by $\log\xi/{\rm erg\,cm\,s^{-1}} = 2.44^{+0.24}_{-0.22}$ and a sulphur column density of $N_{\rm S} = 1.9^{+0.3}_{-0.8} \times 10^{17}\,{\rm cm^{-2}}$. For a solar sulphur/hydrogen

© 2011 The Authors, MNRAS **414,** 3307–3321
Monthly Notices of the Royal Astronomical Society © 2011 RAS

Downloaded from http://mnras.oxfordjournals.org/ at NASA Goddard Space Flight Ctr on July 11, 2014

Table 3. Best-fitting parameters for the fully covering model.

Continuum parameters			
Flux (erg cm^{-2} s^{-1})	$F_{0.5-2.0}$	3.0×10^{-11}	
	$F_{2.0-10.0}$	4.5×10^{-11}	
Luminosity (erg s^{-1})	$L_{0.5-2.0}$	2.83×10^{44}	
	$L_{2.0-10.0}$	4.41×10^{44}	
Best-fitting model components			
Component	Parameter	Value	$\Delta\chi^2$ [g]
Galactic absorption	N_H [a]	2.42×10^{20}	–
cutoffpl	Γ	1.68 ± 0.01	–
	E_{cut} [b]	101^{+23}_{-17}	
reflection	Abund	1*	77.2 [h]
	ξ [d]	<27	
	R	<0.2	
diskbb	T_{in} [c]	62^{+5}_{-6}	114.6
	norm	$2.96^{+1.04}_{-1.32} \times 10^6$	
Soft X-ray absorber 1	N_H [a]	$(5.4 \pm 0.4) \times 10^{20}$	93.7
(Zone 1)	$\log \xi$ [d]	$-0.23^{+0.10}_{-0.12}$	
	v_{out} [e]	300	
	v_{turb} [f]	200	
Soft X-ray absorber 2	N_H [a]	$5.6^{+1.3}_{-2.1} \times 10^{21}$	36.9
(Zone 2)	$\log \xi$ [d]	$2.21^{+0.08}_{-0.07}$	
	v_{out} [e]	300	
	v_{turb} [f]	200	
Fe L absorber	N_H [a]	$5.2^{+6.0}_{-0.9} \times 10^{21}$	74.0
(Zone 3)	$\log \xi$ [d]	$3.02^{+0.08}_{-0.03}$	
	v_{out} [e]	42000^{+3000}_{-5000}	
	v_{turb} [f]	5000	
S XV absorber	N_H [a]	$8.9^{+1.4}_{-3.7} \times 10^{21}$	76.4
(Zone 3)	$\log \xi$ [d]	$2.44^{+0.24}_{-0.22}$	
	v_{out} [e]	6300^{+5100}_{-4200}	
	v_{turb} [f]	1000	
S XVI absorber	N_H [a]	$>1.0 \times 10^{22}$	32.9
(Zone 5)	$\log \xi$ [d]	$3.37^{+0.12}_{-0.41}$	
	v_{out} [e]	19800^{+4200}_{-5100}	
	v_{turb} [f]	1000	

[a] Absorber column density in units of cm^{-2}.
[b] Cut-off energy in units of keV.
[c] Accretion disc blackbody temperature, in units of eV
[d] Ionization parameter in units of erg cm s^{-1}.
[e] Outflow velocity of absorber given in units of km s^{-1}.
[f] Assumed absorber turbulent velocity in units of km s^{-1}.
[g] Significance of component with respect to the final best-fitting model.
[h] Statistical significance of REFLIONX component is given in comparison to a fit where Fe Kα is left unmodelled.
* The parameter was fixed at this value during the fitting process.

abundance ratio of 2.14×10^{-5} (Grevesse & Sauval 1998), this corresponds to a hydrogen column of $N_H = 8.9^{+1.4}_{-3.7} \times 10^{21}$ cm^{-2}, which is similar to the column densities reported previously for this source (i.e. Orr et al. 2001; Kaspi et al. 2004; Gibson et al. 2005, Ramìrez et al. 2008). The net outflow velocity of this absorber is $v_{out} = 6300^{+5100}_{-4200}$ km s^{-1} ($0.021^{+0.017}_{-0.014}$ c), which is consistent with that found when fitting simple Gaussians. At this column density and ionization parameter, the grid also contributes Heβ (1s→3p) and weak Heγ (1s→4p) lines in addition to strong Heα, however the energy separation of the lines is insufficient to fit the line at ∼2.8 keV simultaneously and a second grid is required to model the remaining residuals.

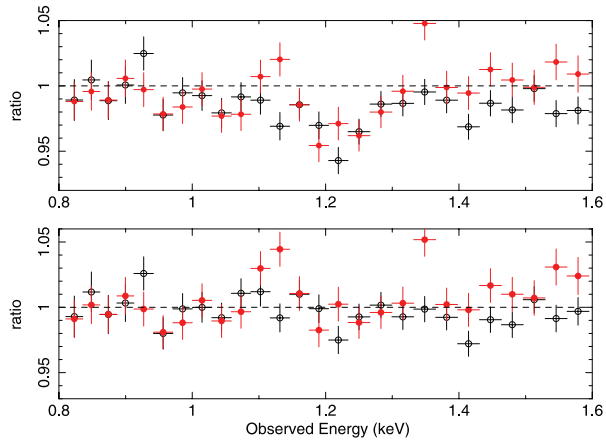

Figure 6. Ratio plots of the 0.8–1.6 keV energy band after the inclusion of absorption Zones 1 and 2. Top: the residual Fe L line profile. Bottom: the same line but when Zone 3 of the photoionization model is added. The residuals are clearly no longer present.

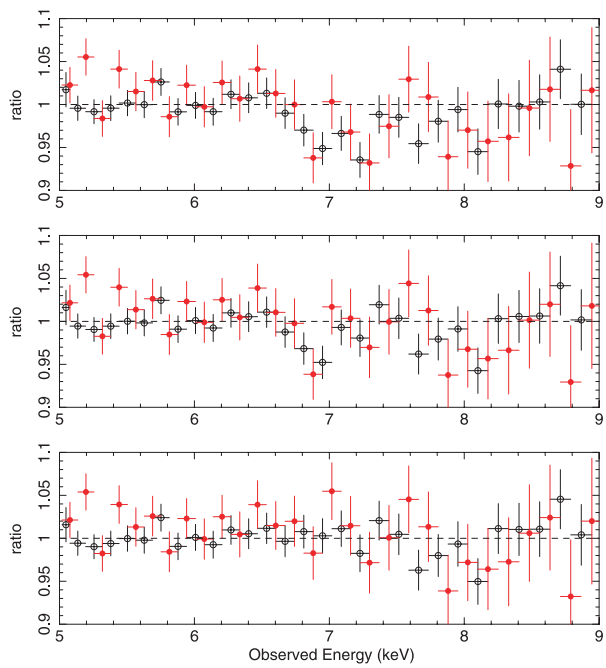

Figure 7. Ratio plots of the Fe K band in the fully covering XSTAR model. Top: when no ionized absorbers are included two residual profiles are apparent between 6.5 and 8.0 keV. Middle: when Zone 3 is added the higher energy residual is no longer present. Bottom: when a further highly ionized zone is added there are no remaining residuals. See text for further details.

The second sulphur absorber (Zone 5; $\Delta\chi^2 = 32.9$) which models the S XVI Lyα is described by $N_S > 2.2 \times 10^{17}$ cm^{-2} ($= N_H > 1 \times 10^{22}$ cm^{-2}) and $\log \xi$/erg cm s^{-1} $= 3.37^{+0.12}_{-0.41}$. The outflow velocity is found to be $v_{out} = 21000 \pm 3000$ km s^{-1} ($0.07 \pm 0.01c$), which is again consistent with that found from simple Gaussian fitting. The fit statistic for the model assuming two zones of Sulphur absorption is χ^2/d.o.f. = 352.2/316.

4.1.4 A further highly ionized zone?

While the soft X-ray and Fe L absorbers contribute a shallow Fe K edge at ∼7.1 keV (see middle panel of Fig. 7) its depth

Downloaded from http://mnras.oxfordjournals.org/ at NASA Goddard Space Flight Ctr on July 11, 2014

insufficient to fit the remaining absorption feature at $E \sim 7.36$ keV (rest frame, observed frame $E \sim 6.92$ keV). This feature can be tentatively ($\Delta\chi^2 = 8.0$ for three additional parameters; Fig. 7 bottom panel) fit by the addition of a $v_{\rm turb} = 5000\,{\rm km\,s^{-1}}$ absorber which is highly ionized, high column density, and is outflowing with $v_{\rm out} = 18000 \pm 3000\,{\rm km\,s^{-1}}$ ($0.06 \pm 0.01c$). The parameters imply that the feature may be identified with Fe XXVI (1s→2p), which is expected to be the must abundant ion at such an ionization. This feature may be a higher velocity analogue of the outflowing Fe XXVI absorption ($v_{\rm out} \sim 12\,700\,{\rm km\,s^{-1}}$) which was reported by Gibson et al. (2005) in a earlier *Chandra*/HETG observation of this source.

4.1.5 *Reflection component*

The above absorbers in addition to the cutoffpl, diskbb and zgauss components provide a good description of the general broad-band continuum and the fit is marginally acceptable (χ^2/d.o.f. = 352.2/316; null probability = 0.08). However, for consistency we replaced the redshifted Gaussian modelling the Fe Kα emission with the ionized reflection model REFLIONX (Ross & Fabian 2005), which self-consistently takes into account any reprocessing due to x-ray reflection in a face-on system. Fixed solar abundances were assumed and the photon index of the reflected power law was tied to that of the intrinsic power law.

The addition of a lowly ionized reflection component ($\xi < 27\,{\rm erg\,cm\,s^{-1}}$) with a low reflection fraction ($R < 0.2$, where $R = \Omega/2\pi$ and Ω is the solid angle subtended by the reflector) reproduces the Fe Kα profile and improves the fit in the hard X-ray band, for a final fit statistic of χ^2/d.o.f. = 342.79/316 (null prob = 0.14), $\Gamma = 1.67^{+0.02}_{-0.03}$ and $E_{\rm cut} = 101^{+30}_{-24}$ keV. The overall best-fitting parameters for the fully covering model are listed in Table 3.

4.2 Partial-covering models

We also investigated the possibility that only a fraction $f < 1$ of the line-of-sight source flux may be covered by the ionized absorbers. This would then require Γ for the power-law continuum to steepen to compensate for the increased absorption. Similar partial-covering scenarios have been invoked to self-consistently model hard X-ray excesses in several AGN (e.g. NGC1365, Risaliti et al. 2009; 1H0419−577, Turner et al. 2009; PDS 456, Reeves et al. 2009). Modelling the hard X-ray excess with partial covering typically requires the intrinsic flux below 10 keV to be strongly absorbed by Compton thick material (i.e. $N_{\rm H} > 10^{24}\,{\rm cm^{-2}}$). However, if the partial coverer is Compton thin, it may also be able to replicate the roll-over and soft excess.

We thus constructed a low turbulence ($v_{\rm turb} = 200\,{\rm km\,s^{-1}}$) partial-covering model using the zxipcf model in XSPEC. Our starting model had the form wabs × (zxipcf×powerlaw+REFLIONX) × XSTAR, where we have removed the diskbb component which previously parametrized the soft excess and reverted to a simple power law with no high-energy cut-off. The overall best-fitting parameters for our partial-covering model are listed in Table 4. Importantly, this model still requires the presence of several fully covering absorbers to account for the Fe L/Fe K and sulphur absorption, and these absorbers have best-fitting parameters which are consistent with those obtained in the fully covering model. A REFLIONX reflection component was also included for self-consistency. In this geometry, the partially covering clouds would need to be very compact in size and located close to the ionizing source to only obscure a fraction of the emergent continuum. One possibility is that the partial coverer may be associated with a clumpy disc wind where the covering fraction relates to the filling factor of the denser clouds, while the more ionized absorbers appear to fully cover the source along the line of sight. Such scenarios have been effective in explaining the broad-band spectral properties of objects such as MCG -6-30-15 (Miller, Turner & Reeves 2008) and 3C 445 (Reeves et al. 2010), and are consistent with theoretical expectations that disc winds are inhomogeneous outflows and contain clumps of dense, high column density, material (e.g. Proga & Kallman 2004; Sim et al. 2010).

In this case the partial-covering model requires a very lowly ionized, high column density absorber which covers approximately 30 per cent of the source in order to fit the soft excess and curvature below 10 keV (Table 4). As expected, the power law is also much

Table 4. Best-fitting parameters for the partial-covering model.

Continuum parameters			
Flux (erg cm^{-2} s^{-1})	$F_{0.5-2.0}$	3.9×10^{-11}	
	$F_{2.0-10.0}$	5.3×10^{-11}	
Luminosity (erg s^{-1})	$L_{0.5-2.0}$	3.88×10^{44}	
	$L_{2.0-10.0}$	5.18×10^{44}	
Best-fitting model components			
Component	Parameter	Value	$\Delta\chi^{2f}$
Galactic absorption	$N_{\rm H}{}^a$	2.42×10^{20}	–
highecut	$E_{\rm cut}$	>244	10.1
Power law	Γ	1.96 ± 0.01	–
Reflection	Abund	1*	54.9^g
	ξ^c	<25	
	R	<0.2	
zxipcf	$N_{\rm H,pcov}$	$(1.2 \pm 0.2) \times 10^{23}$	217.9
	$\log \xi_{\rm pcov}$	$-0.11^{+0.21}_{-0.19}$	
	$f_{\rm cov}$	$0.27^{+0.02}_{-0.03}$	
	$v_{\rm turb}$	200	
Soft X-ray absorber 1	$N_{\rm H}{}^a$	$(7.5 \pm 0.4) \times 10^{21}$	110.3
(Zone 1)	$\log \xi^c$	1.79 ± 0.02	
	$v_{\rm out}{}^d$	<300	
	$v_{\rm turb}{}^e$	200	
Soft X-ray absorber 2	$N_{\rm H}{}^a$	$(2.1^{+0.1}_{-0.3}) \times 10^{21}$	106.3
(Zone 2)	$\log \xi^c$	1.83 ± 0.04	
	$v_{\rm out}{}^d$	27000 ± 3000	
	$v_{\rm turb}{}^e$	$200\,{\rm km\,s^{-1}}$	
Fe L absorber	$N_{\rm H}{}^a$	$4.0^{+0.5}_{-0.6} \times 10^{21}$	48.7
(Zone 3)	$\log \xi^c$	$3.01^{+0.23}_{-0.03}$	
	$v_{\rm out}{}^d$	39000^{+9000}_{-6000}	
	$v_{\rm turb}{}^e$	5000	
S XV absorber	$N_{\rm H}{}^a$	$6.4^{+4.3}_{-2.6} \times 10^{21}$	51.6
(Zone 4)	$\log \xi^c$	$2.47^{+0.19}_{-0.24}$	
	$v_{\rm out}{}^d$	6300 ± 5400	
	$v_{\rm turb}{}^e$	1000	
S XVI absorber	$N_{\rm H}{}^a$	$>6.7 \times 10^{21}$	20.7
(Zone 5)	$\log \xi^c$	$3.37^{+0.18}_{-0.43}$	
	$v_{\rm out}{}^d$	<14000	
	$v_{\rm turb}{}^e$	1000	

[a] Absorber column density in units of cm^{-2}.
[b] Cut-off energy in units of keV.
[c] Ionization parameter in units of erg cm s^{-1}.
[d] Outflow velocity of the absorber given in units of km s^{-1}.
[e] Assumed absorber turbulent velocity in units of km s^{-1}.
[f] Significance of component with respect to the final best-fitting model.
[g] Statistical significance of REFLIONX component is given in comparison to a fit where Fe Kα is left unmodelled.
[*] The parameter was fixed at this value during the fitting process.

Downloaded from http://mnras.oxfordjournals.org/ at NASA Goddard Space Flight Ctr on July 11, 2014

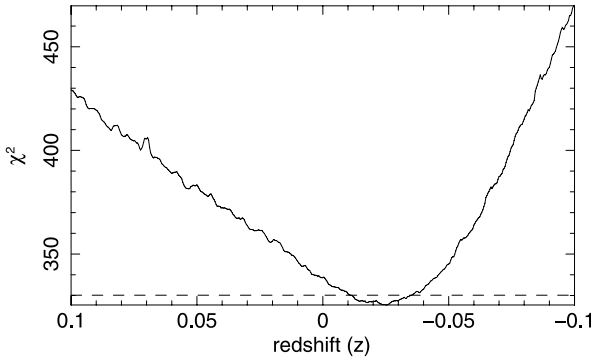

Figure 8. Contour plot of redshift vs fit statistic for the high-velocity soft X-ray absorber in the partial covering model.

steeper ($\Gamma = 1.96 \pm 0.01$) than that usually inferred for this source ($\Gamma = 1.6$–1.7). With just the partial coverer included significant residuals remained in the soft X-ray band and two low turbulence ($v_{\rm turb} = 200\,{\rm km\,s^{-2}}$) fully covering absorbers are also required to achieve an adequate fit (Zones 1 and 2 in Table 4).

Interestingly, the outflow velocity of Zone 2 is $v_{\rm out} = 27\,000 \pm 3000\,{\rm km\,s^{-1}}$ ($0.09 \pm 0.01c$), which is much faster than the 100–1000 km s^{-1} expected for typical WAs (e.g. Crenshaw et al. 2003; Blustin et al. 2005). Nevertheless, the very high outflow velocity is strongly required in this model (see Fig. 8), and fixing the outflow velocity to the source rest frame (i.e. $v_{\rm out} = 0$) resulted in a worse fit by $\Delta\chi^2 = 46.6$ (for one less free parameter). As it is not required in the fully covering scenario, the high outflow velocity of this component is likely to be highly model-dependent and further observations at a higher resolution are required to determine its validity.

4.2.1 *The Fe K band*

As in the fully covering model, the REFLIONX component gives an excellent description of the Fe Kα emission line, and the reflector is once again found to be both lowly ionized and have a low reflection fraction. The partial coverer provides a very good fit to the residual absorption in the Fe K band (see inset of Fig. 9, bottom panel) and, in addition to the Fe XXV Heα absorption which is being modelled by the Fe L absorber, the lowly ionized partial coverer provides an excellent fit to the Fe K edge.

4.2.2 *The high-energy roll-over*

While the overall fit statistic for the partial-covering model is good ($\chi^2 = 335.6/308$; null prob $= 0.13$) the fit still appears to

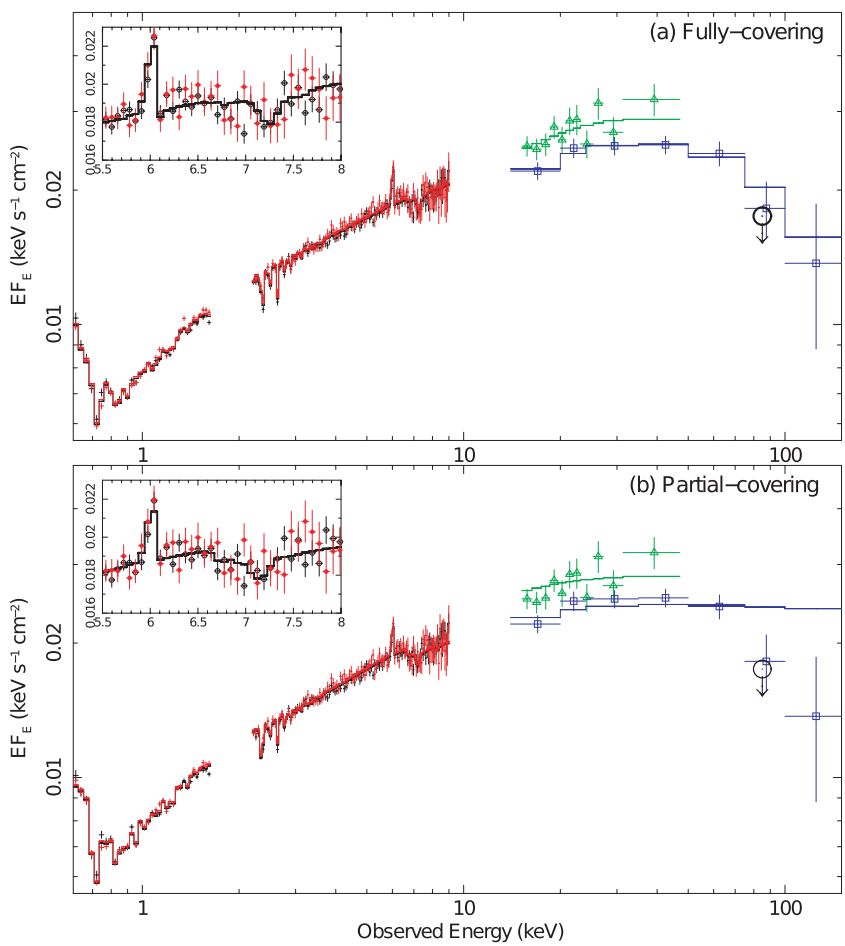

Figure 9. Unfolded best-fitting models for (a) the fully and (b) the partially covering models. Inset in each panel is an enlarged view of the Fe K region of each model. The 1σ upper limit to the HXD/GSO flux is represented by the open circle in both plots and is consistent with the data obtained from the *Swift*/BAT 58 month all-sky survey. Note that we have not included the tentative Fe XXVI component from the inset panel of (a).

Downloaded from http://mnras.oxfordjournals.org/ at NASA Goddard Space Flight Ctr on July 11, 2014

overestimate the flux at the highest energies (see Fig. 9, bottom panel). We thus tried to replicate the roll-over by adding an exponential roll-over using the highecut model; however this only marginally improved the fit ($\Delta\chi^2 = 4.9$ for one additional free parameter). Nevertheless, the final fit statistic for the partial-covering model is χ^2/d.o.f. = 330.7/307 (null hypothesis = 0.168) which is comparable to that obtained with the fully covering model.

5 DISCUSSION

5.1 The soft excess

We have demonstrated that the soft excess in MR 2251−178 can be adequately modelled either as an intrinsic component of the emergent X-ray continuum (i.e. an accretion disc blackbody), or as the side effect of an absorption-dominated (partially covered) spectrum below 10 keV. However, there are several further alternative interpretations which we also considered.

5.1.1 Comptonization

A particular caveat of the fully covering model is the manner in which we have parametrized the soft excess as being the thermal emissions from a geometrically thin accretion disc (diskbb), and thus as an intrinsic component of the X-ray spectrum. While simple and generally well fitting in a wide range of objects, such an interpretation typically requires a thermal continuum with a temperature higher than that expected for geometrically thin accretion discs (e.g. Shakura & Sunyaev 1973; Gierliński & Done 2004; Porquet et al. 2004). The expected temperature for a geometrically thin disc is approximately $T(r) \approx 6.3 \times 10^5 (\dot{M}_{\rm acc}/\dot{M}_{\rm edd})^{1/4} M_8^{-1/4} (r/R_s)^{-3/4}$ K, where M_8 is the accretion disc mass in units of $10^8\,{\rm M}_\odot$. With $(\dot{M}_{\rm acc}/\dot{M}_{\rm edd}) \sim 0.15$ (see later) and $M_8 \sim 2.4$ (Dunn et al. 2008), appropriate for MR 2251−178, and assuming most of the emission originates at the innermost stable circular orbit ($r_{\rm isco} = 3R_{\rm s}$ for a Schwarzschild BH), we have $kT \approx 20$ eV. This is roughly 3 times cooler than the best-fitting diskbb temperature ($kT \sim 62$ eV) and implies that the soft excess cannot easily be attributed to thermal emission from a standard accretion disc without modification.

An alternative interpretation of the soft excess as an intrinsic component is that it is the Wien tail of soft photons from the accretion disc which has been Comptonized by a hot corona located above the plane of the disc (e.g. Czerny & Elvis 1987; Haardt & Maraschi 1991, 1993; Nayakshin, Kazanas & Kallman 2000; Nayakshin 2001). If the distribution of electrons in such a Comptonizing corona is 'quasi-Maxwellian' (i.e. has both a thermal and non-thermal component; see Coppi 1999), it may be able to produce both the hard X-ray power-law continuum for which it is typically invoked, as well as the soft excess.

To see whether this interpretation was feasible, we replaced the diskbb component in our best-fitting fully covering XSTAR model with the COMPTT component (Titarchuk 1994). The thermal temperature of the input accretion disc photons was fixed to $kT \approx 20$ eV, while the redshift was fixed to that of the source. The resulting fit was comparable ($\Delta\chi^2$/d.o.f. = 335.1/308), and the other model parameters were all consistent with that which was obtained previously when using diskbb. The Comptonizing electron temperature is found to be $kT < 5.3$ keV and the optical depth of the corona is $\tau \sim 0.40^{+0.14}_{-0.36}$.

5.1.2 Ionized reflection

A further explanation for the soft excess is as a byproduct of ionized reflection from optically thick matter in the nuclear regions of the AGN, e.g. the accretion disc, the broad line region (BLR) or the molecular torus . However, due to the lack of a strong ionized reflection component and the absence of a broadened iron line, this seems unlikely in the case of MR 2251−178.

5.1.3 Section summary

In summary, the soft excess in MR 2251−178 is well modelled by either a thermal accretion disc blackbody or as the result of the Comptonization of soft thermal photons from the accretion disc. A partial-covering interpretation of the data set is also capable of replicating the soft excess albeit with a steeper power-law photon index, i.e. $\Gamma \sim 2.0$, which is similar to the value found commonly for radio-quiet quasars (e.g. Porquet et al. 2004). The lack of a strong ionized reflection component above 10 keV and the absence of an broadened Fe Kα line suggests than an origin through blurred reflection is unlikely. Regardless of the true nature of the soft excess in MR 2251−178, the parameters that describe the fully covering absorption components are largely invariant between the differing interpretations.

5.2 The Fe Kα line

From past observations of MR 2251−178, there has been significant uncertainty in the reported Fe Kα emission EWs: i.e. 125^{+100}_{-105} eV (*Ginga*; Mineo & Stewart 1993), 190^{+140}_{-95} eV (*ASCA*; Reynolds 1997), 62^{+12}_{-25} eV, (*BeppoSAX*; Orr et al. 2001) 53 ± 20 eV (*XMM–Newton*; Kaspi et al. 2004) and 23^{+14}_{-13} eV (*Chandra*; Gibson et al. 2005).

A possible explanation for the uncertainty is that the previous observations lacked the spectral resolution and S/N in the Fe K band in order to resolve the absorption feature bluewards of the Fe Kα, and this may have artificially broadened the measured EW of the Fe K emission line. Incidentally, we note that the two observations thus far which have reported the presence of Fe XXV/XXVI absorption (this work and Gibson et al. 2005) have also reported the tightest constraint on the Fe Kα EW.

Even so, the Fe Kα EW we find for MR 2251−178 is still below average. For example, based on an archival study of 36 sources in the *Chandra*/HETG archive (which includes MR 2251−178), Shu, Yaqoob & Wang (2010) have reported the narrow core of the Fe Kα emission line has a weighted mean EW of 70 ± 4 eV, which is substantially broader than that which we find here. Furthermore, from their large *Suzaku* study of nearby Seyfert galaxies, Fukazawa et al. (2011) have found that a mean Fe Kα EW of around 55 eV for sources which are absorbed by column densities similar to MR 2251−178 (i.e. $N_{\rm H} \lesssim 10^{22}$ cm^{-2}). Given that MR 2251−178 is a highly X-ray luminous AGN, the apparent weakness of the Fe Kα line could be a result to the 'X-ray Baldwin effect', an apparent anti-correlation between source X-ray luminosity and the Fe Kα EW, which has been well documented in the literature (e.g. Iwasawa & Taniguchi 1993; Page et al. 2004; Jiang, Wang & Wang 2006; see also Fukazawa et al. 2011; Shu et al. 2010). Furthermore, given that MR 2251−178 has a FR I radio morphology, it could also be due to a dilution of the observed X-ray spectrum by a component of X-ray continuum emitted in a radio-jet. The radio-loudness of an object is typically given in terms of the radio-loudness parameter,

Downloaded from http://mnras.oxfordjournals.org/ at NASA Goddard Space Flight Ctr on July 11, 2014

R_L, defined by

$$R_L = \log\left(\frac{F_{5\,\mathrm{GHz}}}{F_{4400\,\mathrm{Å}}}\right), \quad (1)$$

where $F_{5\,\mathrm{GHz}}$ is the monochromatic radio flux at 5 GHz and $F_{4400\,\mathrm{Å}}$; is the optical flux at $\lambda = 4400$ Å. In this regime, objects where $R_L > 1$ are regarded as radio-loud, while those where $R_L < 1$ are radio-quiet. For MR 2251−178, Reeves & Turner (2000) found that $R_L = -0.43$, which suggests that any present radio-jet is very weak and unlikely to contribute in the X-ray band.

Finally, it is also possible that the weakness of the Fe Kα emission may be due to the inner accretion disc being shielded by the outflow. If this is the case, this could also explain the lack of a strong ionized reflection component as the observed reflection would have to originate at distances further from the central engine, i.e. the BLR or the torus. Sim et al. (2010) have recently shown that Fe Kα emission can originate via reflection from dense material in an outflowing wind (with EWs∼10 s of eV), which may possibly be applicable in MR 2251–178. Furthermore, the Fe Kα EW can also become suppressed in the presence of a sufficiently high column absorber (e.g. Miller et al. 2010; Yaqoob et al. 2010) such as those found here.

5.3 The multicomponent outflow of MR 2251–;178

We have shown that the X-ray spectrum of MR 2251−178 can be adequately modelled with both a fully covering and an absorption-dominated partial-covering interpretation. We find that both of these models require the presence of a number of fully covering absorbers to account for the observed Fe UTA, Fe L (Fe XXIII–XXIV), S XV, S XVI and Fe XXV–XXVI absorption lines. In this section, we turn our attention to these absorbers and investigate their geometries, kinematics and, ultimately, estimate their energetic output. For simplicity, we consider here the absorbers as per the fully covering model, and focus on the Fe L absorber as it is likely to be the most energetic given its high v_{out}. For completeness, however, the methods discussed here were individually applied to all absorbers in the fully covering model and the results are summarized in Table 5.

Note that as the parameters of the Fe L absorber are largely invariant between the two models, the results obtained here are applicable to either interpretation and are thus not model-dependent.

5.3.1 *Distance*

The observed column density of a spherically symmetric absorber a distance R from the ionizing source is equal to the absorber density multiplied by the thickness of the shell of material, i.e. $N_{\mathrm{H}} \approx n\delta R$. From the definition of the ionization parameter, $\xi = L_{\mathrm{ion}}/nR^2$, where L_{ion} is the ionizing luminosity between 1 and 1000 Rydbergs (from 13.6 eV to 13.6 keV) and n is the hydrogen gas density, this then implies that the inner face of the absorber, R, is located at

$$R = \frac{L_{\mathrm{ion}}}{\xi\, N_{\mathrm{H}}}\left(\frac{\delta R}{R}\right) \quad (2)$$

from the central ionizing continuum. Assuming that the absorber forms a thin shell where $\delta R/R < 1$, equation (2) then sets an upper limit on the distance to the inner face of the absorbing material, i.e. $R < L_{\mathrm{ion}}/\xi N_{\mathrm{H}}$. From the best-fitting continuum parameters of the fully covering model, L_{ion} is estimated to be of the order of 2×10^{45} erg s^{-1}. Therefore, taking $N_{\mathrm{H}} \sim 5.2 \times 10^{21}$ cm^{-2} and $\log \xi/\mathrm{erg\,cm\,s^{-1}} \sim 3.0$ characteristic of the Fe L absorber, we find $R \lesssim 100$ pc.

Assuming that the outflow escapes the system we can set a lower limit on the radial distance by considering the escape radius of the material. For a spherical geometry, the radius at which material will be able to escape the BH is given by

$$R_{\mathrm{esc}} \geq \frac{2GM}{v_{\mathrm{out}}^2} \approx \left(\frac{2c^2}{v_{\mathrm{out}}^2}\right) R_{\mathrm{g}}, \quad (3)$$

with $R_{\mathrm{g}} \equiv GM/c^2$ being the gravitational radius. Given that the Fe L absorber has an outflow velocity of $\sim 0.14c$, $R_{\mathrm{esc}} \gtrsim 100 R_{\mathrm{g}}$. This suggests that the outflow may have an origin consistent with an accretion disc wind or the BLR. Indeed, Kaspi et al. (2004) set a lower limit on the size of the BLR in MR 2251−178 of 0.04 ± 0.01 pc ($\approx 3000\,R_{\mathrm{g}}$), which has significant overlap with the upper limit obtained here.

5.3.2 *Mass outflow rates*

We can also estimate the mass outflow rate. Assuming a quasi-spherical system:

$$\dot{M}_{\mathrm{out}} = 4\pi b R^2 n_{\mathrm{e}} m_{\mathrm{p}} v_{\mathrm{out}} \quad (4)$$

$$\approx 4\pi b \left(\frac{L_{\mathrm{ion}}}{\xi}\right) m_{\mathrm{p}} v_{\mathrm{out}}, \quad (5)$$

where $b \equiv \Omega/4\pi \leq 1$ is the geometrical factor allowing for an outflowing wind subtending solid angle Ω. The parameters of the Fe L absorber suggest that it is capable of expelling $\sim 2700b\,\mathrm{M_\odot\,yr^{-1}}$. For comparison, the accretion rate required to maintain the observed radiative bolometric output is

$$\dot{M}_{\mathrm{acc}} = \frac{L_{\mathrm{bol}}}{\eta c^2}, \quad (6)$$

where L_{bol} is the bolometric luminosity and η is the accretion efficiency. With $\eta = 0.06$ for a Schwarzschild BH accreting at

Table 5. Summary of absorption zone parameters.

	Soft X-ray 1 (Zone 1)	Soft X-ray 2 (Zone 2)	S XV (Zone 3)	S XVI (Zone 3)	Fe L/Fe K (Zone 5)
v_{out} (km s^{-1})	300*	300*	6300^{+5100}_{-4200}	19800^{+4200}_{-5100}	42000^{+3000}_{-5000}
R (pc)	2×10^6	700	300	30	100
R_{esc} (pc)	20	20	0.06	0.005	0.001
$\dot{M}_{\mathrm{out}}$ (M$_\odot$ yr^{-1})	$33000b$	$100b$	$1500b$	$600b$	$2700b$
b	10^{-5}	10^{-3}	10^{-2}	10^{-3}	10^{-3}
$\dot{E}_{\mathrm{out}}$ (erg s^{-1})	$\sim 10^{45}b$	$\sim 10^{42}b$	$\sim 10^{46}b$	$\sim 10^{46}b$	$\sim 10^{48}b$
$\dot{E}_{\mathrm{out(corr)}}$ (erg s^{-1})	$\sim 10^{40}$	$\sim 10^{39}$	$\sim 10^{44}$	$\sim 10^{43}$	$\sim 10^{45}$

*Denotes that the parameter was fixed at this value.

Downloaded from http://mnras.oxfordjournals.org/ at NASA Goddard Space Flight Ctr on July 11, 2014

maximum efficiency, and adopting an UV-determined bolometric luminosity of 4.3×10^{45} erg s^{-1} (Dunn et al. 2008), we find that the AGN in MR 2251−178 requires an accretion rate of $\dot{M}_{\rm acc} \sim 1.3\,{\rm M}_{\odot}\,{\rm yr}^{-1}$ to maintain its bolometric radiative output. This is orders of magnitude lower than the estimated mass outflow rate and implies that either (1) the AGN will exhaust its fuel supply of accreting material over a relatively short time-scale in order to maintain an effective mass outflow rate much higher than $\dot{M}_{\rm acc}$ or (2) the outflow is not spherical and has a small covering fraction or is rather clumpy (i.e. $b \ll 1$). Similar conclusions were also reached by Gibson et al. (2005) in their analysis of the *Chandra*/HETG observation.

By assuming that $\dot{M}_{\rm out} \lesssim \dot{M}_{\rm acc}$, we can estimate the clumping/covering b factor of the outflow with respect to the central nucleus, i.e. $b \approx \dot{M}_{\rm acc}/\dot{M}_{\rm out} \approx 10^{-3}$. The resulting inferred covering factors are listed in Table 5. We note that in principle b could be larger than this. However, this estimate allows us to set a conservative lower limit to the energetics of the outflow in the next section.

5.3.3 *Energetics*

The kinetic luminosity of the Fe L absorber is

$$\dot{E}_{\rm out} = \frac{1}{2}\dot{M}_{\rm out} v_{\rm out}^2 b \sim 10^{48} b\,{\rm erg\,s^{-1}} \quad (7)$$

which implies a conservative mechanical output of $\sim 10^{45}$ erg s^{-1} for $b \sim 10^{-3}$ as discussed above. This makes the Fe L absorber the most significant outflowing component in terms of overall energetics, despite its substantial putative clumping. The energetics of the other absorbers are listed in Table 5.

Assuming that the BH mass grows through accretion alone, we can then estimate a required 'active phase' for the quasi-stellar object as the current estimated BH mass (2.4×10^8 M$_{\odot}$) divided by the accretion rate, i.e. $\sim 10^8$ yr. Combining this with the mechanical output calculated previously suggests that the Fe L absorber has an estimated mechanical output of $\sim 10^{60}$ erg over the lifetime of the AGN. This is comparable to the binding energy of a typical 10^{11} M$_{\odot}$ galaxy bulge and further supports the premise that such outflows may be energetically significant in AGN/Galaxy feedback scenarios.

6 SUMMARY

We have performed a broad-band spectral analysis of the radio-quiet quasar MR 2251−178 using recent observations from *Suzaku* and the *Swift*/BAT. Below is a summary of our results.

(i) The continuum shows considerable curvature above around ∼10 keV and an apparent soft excess is present below 1 keV. A weak (EW = 26^{+16}_{-6} eV), unresolved ($\sigma < 117$ eV), Fe Kα emission line from neutral material is present at ∼6.4 keV. The spectral curvature and soft excess can be equally well modelled as an artefact of an absorption-dominated, partially covered, continuum or as a fully covered intrinsic continuum component.

(ii) Absorption lines due to the Fe UTA and the Fe L-shell are present below 2 keV. The Fe L line is consistent with being a blueshifted blend of 2s→3p transitions from Fe XXIII and Fe XXIV. Two further absorption lines are detected at ∼2.5 and ∼2.8 keV, which we conservatively identify with S XV Heα and S XVI Lyα. For this identification the lines require blueshifted velocities of $\sim 0.02c$ and $\sim 0.07c$, respectively. From Monte Carlo (MC) simulations, we find that all soft X-ray absorption lines are significant at the >99.9 per cent level.

(iii) We also detect significant (99.3 per cent from MC) absorption in the Fe K band ($E \sim 7.5$ keV; rest frame) which is consistent with the presence of blueshifted Fe XXV–XXVI. A single high turbulence ($v_{\rm turb} = 5000$ km s^{-1}) ionized absorber provides a good fit to both the Fe L-shell line at ∼1.29 keV and to a portion of the absorption present in the Fe K band, requiring an outflow velocity of $v_{\rm out} \sim 0.14c$.

(iv) We derive distances to the absorbers and find that the Fe L absorption may originate at subparsec scales, possibly in an accretion disc wind. By balancing the mass outflow and mass accretion rates, we estimate covering fractions (or 'clumpiness') and subsequent energetics for all absorbers. The Fe L absorber is consistent with being substantially clumped, by a factor of around 10^{-3}, but still dominates in terms of the overall energetics with a conservatively estimated kinetic output of $\sim 10^{45}$ erg s^{-1}.

ACKNOWLEDGMENTS

The *Suzaku X-ray observatory* is a collaborative mission between the Japan Aerospace Exploration Agency (JAXA) and the National Aeronautics and Space Administration (NASA). This research has made use of the NASA/IPAC Extragalactic Data base (NED) which is operated by the Jet Propulsion Laboratory, Caltech, under contract with the NASA. We would like to thank the anonymous referee for their comments on this work, and Dean McLaughlin for his suggestions. JG and VB would like to acknowledge support from the UK STFC research council.

REFERENCES

Arnaud K. A., 1996, in Jacoby G., Barnes J., eds, ASP Conf. Ser. Vol. 101, Astronomical Data Analysis Software and Systems V. Astron. Soc. Pac., San Francisco, p. 17
Baumgartner W. H. et al., 2010, ApJS, submitted
Bautista M. A., Kallman T. R., 2001, ApJS, 134, 139
Behar E., Sako M., Kahn M. S., 2001, ApJ, 563, 497
Bergeron J., Bennefeld M., Boksenberg A., Tarenghi M., 1983, MNRAS, 202, 125
Blustin A. J., Page M. J., Fuerst S. V., Branduardi–Raymont G., Ashton C. E., 2005, A&A, 431, 111
Boldt E., 1987, in Hewitt A., Burbridge G., Fang L. Z., eds, IAU Symp. 124, Observational Cosmology. Reidel, Dordrecht, p. 611
Braito V. et al., 2007, ApJ, 670, 978
Braito V., Reeves J. N., Sambruna R., Gofford J., 2011, MNRAS, doi:10.1111/j.1365-2966.2011.18590.x
Canizares C. R., McClintock J. E., Ricker G. R., 1978, ApJ, 226, 1
Cappi M. et al., 2009, A&A, 504, 401
Chartas G., Eracleous M., Dai X., Agol E., Gallagher S., 2007, ApJ, 661, 678
Cooke B. A. et al., 1978, MNRAS, 182, 489
Coppi P. S., 1999, in Poutanen J., Svensson R., eds, ASP Conf. Ser. Vol. 161, High Energy Processes in Accreting Blank Holes. Astron. Soc. Pac., San Francisco, p. 375
Crenshaw D. M., Kraemer S. B., George I. M., 2003, ARA&A, 41, 117
Czerny B., Elvis M., 1987, ApJ, 321, 305
Dickey J. M., Lockman F. J., 1990, ARA&A, 28, 215
Dunn J. P., Crenshaw D. M., Kraemer S. B., Tripple M. L., 2008, AJ, 136, 1201
Ferrarese L., Merritt D., 2000, ApJ, 539, 9

Downloaded from http://mnras.oxfordjournals.org/ at NASA Goddard Space Flight Ctr on July 11, 2014

Fukazawa Y., Mizuno T., Watanabe S., Kokubun M., Takahashi H. et al., 2009, PASJ, 61, S17
Fukazawa Y. et al., 2011, ApJ, 727, 19
Ganguly R., Charlton J. C., Eracleous M., 2001, ApJ, 556, 7
Gebhardt K. et al., 2000, ApJ, 539, 13
Gibson R. R., Marshall H. L., Canizares C. R., Lee J. C., 2005, ApJ, 627, 83
Gierliński M., Done C., 2004, MNRAS, 349, 7
Grevesse N., Sauval A. J., 1998, Space Sci. Rev., 85, 161
Haardt F., Maraschi L., 1991, ApJ, 380, 51
Haardt F., Maraschi L., 1993, ApJ, 413, 507
Halpern J. P., 1984, ApJ, 281, 90
Iwasawa K., Taniguchi Y., 1993, ApJ, 413, 15
Jiang P., Wang J. X., Wang T. G., 2006, ApJ, 644, 725
Kaastra J. S., Mewe R., Liedahl D. A., Komossa S., Brinkman A. C., 2000, A&A, 354, 83
Kallman T. R., McCray R., 1982, ApJS, 50, 263
Kallman T. R., Palmeri P., Bautista M. A., Mendoza C., Krolik J. H., 2004, ApJS, 155, 675
Kaspi S. et al., 2002, ApJ, 574, 643
Kaspi S., Netzer H., Chelouche D., George I. M., Nandra K., Turner T. J., 2004, ApJ, 611, 68
King A. R., 2003, ApJ, 596, L27
King A. R., 2010, MNRAS, 402, 1516
Koyama K. et al., 2007, PASJ, 59, 23
McKernan B., Yaqoob T., Reynolds C. S., 2007, ApJ, 379, 1359
Miller L., Turner T. J., Reeves J. N., George I. M., Kraemer S. B., Wingert B., 2007, A&A, 463, 131
Miller L., Turner T. J., Reeves J. N., 2008, A&A, 483, 437
Miller L., Turner T. J., Reeves J. N., Braito V., 2010, MNRAS, 408, 1928
Mineo T., Stewart G. C., 1993, MNRAS, 262, 817
Mitsuda K. et al., 2007, PASJ, 59, 1
Monier E. M., Mathur S., Wilkes B., Elvis M., 2001, ApJ, 559, 675
Morrison R., McCammon D., 1983, ApJ, 270, 119
Nayakshin S., 2001, Advances Space Res., 28, 425
Nayakshin S., Kazanas D., Kallman T. R., 2000, ApJ, 537, 833
Netzer H., 2004, ApJ, 604, 551
Orr A., Barr P., Guainazzi M., Parmar A., Young A., 2001, A&A, 376, 413
Page K. L., O'Brien P. T., Reeves J. N., Turner M. J. L., 2004, MNRAS, 347, 316
Pan H. C., Stewart G. C., Pounds K. A., 1990, MNRAS, 242, 177
Phillips M. M., 1980, ApJ, 236, 45
Porquet D., Reeves J. N., O'Brien P., Brinkmann W., 2004, A&A, 422, 85
Pounds K. A., Reeves J. N., 2007, MNRAS, 374, 823
Pounds K. A., Reeves J. N., King A. R., Page K. L., O'Brien P. T., Turner M. J. L., 2003, MNRAS, 345, 705
Proga D., Kallman T. R., 2004, ApJ, 616, 688
Ramìrez J. M., Komossa S., Burwitz V., Mathur S., 2008, ApJ, 681, 965
Reeves J. N., Turner M. J. L., 2000, MNRAS, 316, 234
Reeves J. N., O'Brien P. T., Ward M. J., 2003, ApJ, 593, 65
Reeves J. N. et al., 2009, ApJ, 701, 493
Reeves J. N., Gofford J., Braito V., Sambruna R. M., 2010, ApJ, 725, 803
Reynolds C. S., 1997, MNRAS, 286, 513
Ricker G. R., Clark G. W., Doxsey R. E., Dower R. G., Jernigan J. G., Delvaille J. P., MacAlpine G. M., Hjellming R. M., 1978, Nat, 271, 35
Risaliti G., Bianchi S., Matt G., Baldi A., Elvis M., Fabbiano G., Zezas A., 2005, ApJ, 630, 129
Risaliti G. et al., 2009, ApJ, 705, 1
Ross R. R., Fabian A. C., 2005, MNRAS, 358, 211
Shakura N. I., Sunyaev R. A., 1973, A&A, 24, 337
Shu X. W., Yaqoob T., Wang J. X., 2010, ApJS, 187, 581
Sim S. A., Proga D., Miller L., Long K. S., Turner T. J., 2010, MNRAS, 408, 1396
Spergel D. N. et al., 2003, ApJS, 148, 175
Takahashi T. et al., 2007, PASJ, 59, 35
Titarchuk L., 1994, ApJ, 434, 570
Tombesi F., Cappi M., Reeves J. N., Palumbo G. G. C., Yaqoob T., Braito V., Dadina M., 2010a, A&A, 521, 57
Tombesi F., Sambruna R. M., Reeves J. N., Braito V., Ballo L., Gofford J., Cappi M., Mushotzky R. F., 2010b, ApJ, 719, 700
Turner T. J., Reeves J. N., Kraemer S. B., Miller L., 2008, A&A, 483, 161
Turner T. J., Miller L., Kraemer S. B., Reeves J. N., Pounds K. A., 2009, ApJ, 698, 99
Yaqoob T., Murphy K. D., Miller L., Turner T. J., 2010, MNRAS, 401, 411

APPENDIX A: LINE IDENTIFICATIONS

The outflow velocities (and resultant energetics) of the absorbers are contingent on the correct identifications of the absorption features. Most of the absorption features detected in the *Suzaku* spectrum have rest-frame energies which do not correspond to any strong features expected in the X-ray band, and have thus been conservatively identified as being the blueshifted absorption from the strongest expected nearby spectral transition. Here we discuss alternative identifications for these absorption lines.

A1 Fe XXIV

The observed energy range of the suspected Fe XXIV (2s→3p) line, i.e. 1.28–1.30 keV, is populated by an array of high-order transitions from low-abundance elements which makes a rest-frame identification unlikely. For example, the 2s→*n*d transitions of Co XVIII and Co XX are found in this energy range which can be ruled out based on its very low astrophysical abundance (i.e. Co/H $\sim 10^{-8}$). Indeed, these transitions are also unlikely as they are expected to be very weak in comparison to their lower order counterparts.

The line is also unlikely to be identified with any blueshifted lines from the expected abundant elements (i.e. O, Ne) without an extreme outflow velocity. For example, if identified with H- or He-like neon (1.02 and 0.922 keV, respectively) the outflow velocity would be $\sim$0.3–0.4c. This is much larger than that typically found in AGN WAs (e.g. Blustin et al. 2005). Furthermore, an identification with the 1s→2p lines of Na X/XI (1.12 and 1.24 keV) is unlikely as such Na absorption has not been reported in even the longest exposure AGN X-ray spectra (e.g. Kaspi et al. 2002).

As an identification with any local 1s→2p transition is unlikely, we also considered nearby 2s→3p transitions. The most likely 2s→3p transitions local to the $\sim$1.29 keV line are that of Fe XXIV at $\sim$1.165 keV. For this identification, the line would then require an outflow velocity of $\sim$0.1c. We note that while the oscillator strengths of the 2s→3p lines of Fe XXV (expected at E1.22–1.24 keV) are expected to be higher than those of Fe XXIV in this band, the required outflow velocity assuming this identification ($v_{\rm out}$0.04–0.06c) would be incompatible with that obtained from XSTAR fitting (see Section 4.1.2).

A2 S XV/XVI

The lines at $E = 2.52 \pm 0.02$ and 2.79 ± 0.03 keV do not correspond with any expected transitions in the rest frame. The only transitions which have consistent rest-frame energies are those associated with extremely low abundance elements which are not expected to be observed in the X-ray spectrum (e.g. Kr, Rb, Mo).

The higher energy line is consistent with the 1s→3p He-like sulphur line at $E \sim 2.88$ keV, but such an identification is again unlikely given that at the best-fitting ionization stage (Table 3) H-like sulphur is expected to be the dominant ion (Kallman & McCray 1982). Furthermore, if the line was caused by the He-like sulphur 1s→3p line, we would still expect to see much stronger 1s→2p transitions, which are not present. Thus a $v_{\rm out} = 0$ origin appears

Downloaded from http://mnras.oxfordjournals.org/ at NASA Goddard Space Flight Ctr on July 11, 2014

to be ruled out for both of the lines and they are most likely to be blueshifted.

The most likely ions in the 2–3 keV energy band which are expected to be strong in the X-rays are He- and H-like sulphur at $E = 2.461$ and 2.623 keV, respectively. An identification with silicon (e.g. Si XIV Lyα at 2.01 keV) would require a substantially larger soft X-ray outflow velocity $v \sim 0.2-0.4c$ and thus seems unlikely; as does an identification with any lower Z ions for similar reasons.

A3 Fe XXV/XXVI

While their oscillator strengths suggest that the absorption features between 7 and 8 keV are most likely Fe XXV/XXVI, several other elements are also expected to have transitions above ∼7 keV which may interfere with this identification. Most notable of these are H- and He-like nickel which have 1s→2p lines at rest-frame energies of ∼7.8 and ∼8.1 keV, respectively. The observed energy of the absorption feature is consistent with neither of these transitions without significant redshift, however, making an identification unlikely. An identification with lower ionization nickel could be plausible, but the column densities at which moderately ionized nickel would be observed are unacceptably high (i.e. $N_{\rm H} > 10^{24}$ cm^{-2}) and, with an abundance ratio of Fe/Ni∼20 (Grevesse & Suvaul 1998), one would also expect to observe hugely dominant 1s→2p Fe transitions, which are not observed. Thus an identification with Ni would appear to be ruled out.

For the tentative high-ionization Fe K absorber, an identification with any ions other than Fe XXVI is unlikely given the high ionization (Kallman et al. 2004). Furthermore, while Zone 5 may be contributing Fe XXIII–XXIV 1s→2p lines to the Fe K band, Fe XXV is expected to be the dominant ion at the measured ionization parameter, and we adopt it as our most probable line identification for the contribution of Zone 5 to the Fe K band.

This paper has been typeset from a TEX/LATEX file prepared by the author.

Downloaded from http://mnras.oxfordjournals.org/ at NASA Goddard Space Flight Ctr on July 11, 2014